Analysis of laser surgery in non-melanoma skin cancer for optimal tissue removal

Félix Fanjul-Vélez, Irene Salas-García, José Luis Arce-Diego

Applied Optical Techniques Group, Electronics Technology, Systems and Automation Engineering Department, University of Cantabria, Av. de los Castros s/n, 39005 Santander (Spain)

E-mail: fanjulf@unican.es; arcedj@unican.es

Abstract. Laser surgery is a commonly used technique for tissue ablation or resection of malignant tumors. It presents advantages over conventional non-optical ablation techniques, like a scalpel or electrosurgery, such as the increased precision of the resected volume, scars minimization, or shorter recovery periods. Laser surgery is employed in medical branches such as ophthalmology or dermatology. The application of laser surgery requires the optimal adjustment of laser beam parameters, taking into account the particular patient and lesion. In this work we present a predictive tool for tissue resection in biological tissue after laser surgery, which allows an a priori knowledge of the tissue ablation volume, area and depth. The model employs a Monte Carlo 3D approach for optical propagation, and a rate equation for plasma-induced ablation. The tool takes into account characteristics of the specific lesion to be ablated, mainly the geometric, optical and ablation properties. It also considers the parameters of the laser beam, such as radius, spatial profile, pulse width, total delivered energy or wavelength. The predictive tool is applied to dermatology tumor resection, particularly to different types of non-melanoma skin cancer tumors: basocellular carcinoma, squamous cell carcinoma and infiltrative carcinoma. The ablation volume, area and depth are calculated for healthy skin and for each type of tumor as a function of laser beam parameters. The tool could be used for laser surgery planning before the clinical application. The laser parameters could be adjusted for optimal resection volume, by personalizing the process to the particular patient and lesion.

1. Introduction

Optical techniques provide several advantages in biomedical applications, such as the non-invasive, non-contact character, and the use of non-ionizing radiation (Vo-Dinh 2003), including diagnosis, treatment of diseases, such as Photodynamic Therapy (PDT) (Salas-García *et al* 2012a), and surgery. The application of lasers to surgery is a quite extended medical procedure, either for tissue resection or as an optical scalpel (Niemz 2004, Vogel and Venugopalan 2003).

The use of laser radiation for biological tissue ablation is routinely employed since the mid-1980s (Vogel and Venugopalan 2003). Nowadays laser surgery is quite extended in several medical specialties, such as dentistry, otolaryngology, gastroenterology, ophthalmology or dermatology (Peng *et al* 2008). Laser surgery provides several advantages compared with conventional scalpels, electrosurgery, ultrasonic or RF ablation, such as the precision of the resected volume, the minimization of scars, or the shorter recovery periods (Sankaranarayanan *et al* 2013). Laser types most frequently employed are the Nd:YAG, Argon, PDL or CO2 (Sankaranarayanan *et al* 2013).

Laser surgery is commonly used in dermatology, by means of the pulsed dye laser (PDL), ruby, KTP, alexandrite, Nd:YAG or CO_2, among others (Peng *et al* 2008, Alexandrescu and

Ross 2012). Skin cancer tissue removal by laser surgery provides a non-invasive method, the possibility of applying the treatment in sensible locations, and a good cosmetic result (Alexandrescu and Ross 2012). PDT can also be applied to skin cancer or even precursor lesions, like actinic keratosis (Salas-García *et al* 2012b). Previous clinical results of the application of PDT in the Dermatology Service of the Marqués de Valdecilla University Hospital (Santander, Spain) show a recurrence rate of between 3 and 6% (Fanjul-Vélez *et al* 2009a). This is mainly due to inefficient PDT patient- and lesion-independent protocol application, and also to large tumor volume. As an alternative ablative laser surgery is employed for several skin cancer or even precursor lesions, such as CO2 or Er:YAG lasers for actinic keratosis, basocellular and squamous cells carcinomas, or PDL for basocellular carcinomas (Choudhary *et al* 2011). Clinical studies show variable recurrence rates in specific applications, from no recurrence to even 13% after one year (Choudhary *et al* 2011).

The application of laser surgery for tumor resection requires an adequate control of the ablated volume. Laser parameters such as wavelength, irradiance, pulse width, repetition rate or spatial profile, and lesion-dependent parameters influence the final resected tumor volume. In this work we present a novel predictive tool for the estimation of the resected volume of several skin cancer lesions by laser surgery. The tool takes into account the parameters of the particular lesion, specifically the optical and ablation properties, and those of the laser source, particularly wavelength, irradiance, spatial profile or pulse width. The proposed model considers the complex irradiation pattern of light in turbid media, and the 3D geometry of the problem, on the contrary of usual models (Vo-Dinh 2003). The predictive model is applied to three nonmelanoma skin cancer types: squamous cells carcinoma, basocellular carcinoma and infiltrative carcinoma. The article is organized as follows. Section 2 is devoted to a brief description of the lesions. Section 3 contains the details of the optical propagation model employed. In section 4 the ablation approach is analyzed. Section 5 presents the results of the application to different lasers and lesions. In section 6 the main conclusions of this work are exposed.

2. Nonmelanoma skin cancer

The most common type of cancer in Western countries is nonmelanoma skin cancer, which accounts for approximately one third of all diagnosed cancers (Choudhary *et al* 2011). It represents around 80% of the total amount of cutaneous cancers, with an apparition rate 20 times that of the melanoma. Among all these cases of nonmelanoma skin cancer, Basal Cell Carcinoma (BCC) represents more than one half. Nonmelanoma skin cancer includes also pathologies such as Squamous Cell Carcinoma (SCC) or Infiltrative Carcinoma (INF). In terms of expenditure of the health system, nonmelanoma skin cancer is the fifth costliest cancer (Choudhary *et al* 2011).

Figure 1. Images of Basal Cell Carcinomas (BCC). Marqués de Valdecilla University Hospital.

BCC appears in basal cells, usually originated without a previous lesion. Metastasis risk is extremely low, but this kind of cancer is able to provoke great local tissue destruction (Diepgen and Mahler 2002). Figure 1 shows two images of BCCs from the Marqués de Valdecilla University Hospital. SCC appears in the epidermis of skin and presents a fast growing process, so it is more likely to invade other tissues. SCC is usually successfully treated by surgical removal. However, some aggressive cases provoke extended tissue destruction and metastasis, in around 5% of the cases, and finally death. Previous lesions that

degenerate in squamous cell carcinoma are actinic keratosis and Bowen disease (Diepgen and Mahler 2002). Figure 2 shows images of actinic keratosis and Bowen disease from Marqués de Valdecilla University Hospital. INF is the most invasive one. This cancer grows over the cell layer where it first appeared. It is common in mammalian cancer.

Nonmelanoma skin cancer is usually caused by an accumulated solar ultraviolet exposition, although the origin is greatly varying. The incidence of nonmelanoma skin cancer is increasing by 4% each year. This great increase is thought to be related with some habits like the increasing amount of solar exposition, the change in clothing habits, the increased longevity and the reduction of ozone in the atmosphere (Fanjul-Vélez *et al* 2009b).

Figure 2. Images of actinis keratosis (left) and Bowen disease (right). Marqués de Valdecilla University Hospital.

Cure and cosmetic results are the main objectives of the treatment, as the most usual areas affected by nonmelanoma skin cancer are the exposed body parts, like the face, and due also to the low death rate. The treatment must be oriented to tumour elimination, recurrence avoidance, recovery of the cosmetic and functional appearance of skin and maximization of the rate cost-effectiveness. Laser ablative surgery is a good approach to this aim.

3. Optical propagation in biological tissues

The analysis of laser surgery requires first the study of optical propagation of laser radiation in nonmelanoma skin cancer, as ablation depends strongly on it (Niemz 2004).

The calculation of light propagation in highly heterogeneous media like biological tissues can be done by means of several approaches (Fanjul-Vélez and Arce-Diego 2008). Analytical solutions of Maxwell equations are only available for simple geometries (Bohren and Huffman 1983). Other models consider the real tissue as a ground material with randomly located spheres of another material, such as the two fluxes Kubelka-Munk model (Vo-Dinh 2003), a seven fluxes approach, or an exponential 1D approach (Fanjul-Vélez and Arce-Diego 2008).

In this work a 3D model based on the Radiation Transport Theory (RTT) (Vo-Dinh 2003) is employed. The basic parameter is the specific intensity, $I(r,\hat{s})$, light power per unit area per unit solid angle. Scattering is described by the scattering phase function $p(\hat{s}\cdot\hat{s}')$. The general Radiation Transport Equation in a medium with no sources and steady-state is:

$$\hat{s}\cdot\overline{\nabla}I(r,\hat{s}) = -(\mu_a+\mu_s)I(r,\hat{s}) + \frac{\mu_s}{4\pi}\int_{4\pi} p(\hat{s}\cdot\hat{s}')\,I(r,\hat{s})d\Omega' \quad (1)$$

Equation 1 can be solved analytically for limiting cases, such as dominant attenuation or dominant scattering (Vo-Dinh 2003). Numerical analysis of an arbitrary biological tissue can be also employed, like the Monte Carlo method (Fanjul-Vélez and Arce-Diego 2008). The implementation by Wang *et al* (1995) assumes cylindrical symmetry and it is multi-layered, so several plane-parallel layers of different composition can be defined. This situation is very common in biological tissues.

The Monte Carlo method employs optical properties and dimensions of the different layers of the biological tissues: the refractive index n, the absorption coefficient $\mu_a(m^{-1})$, the

scattering coefficient $\mu_s(m^{-1})$, and the anisotropy of scattering g (dimensionless). The latter is related with the scattering phase function by:

$$g = \frac{\int_{4\pi} p(\hat{s}\cdot\hat{s}\prime)\hat{s}\cdot\hat{s}\prime d\Omega\prime}{\int_{4\pi} p(\hat{s}\cdot\hat{s}\prime)d\Omega\prime} = \frac{1}{4\pi W_0}\int_{4\pi} p(\hat{s}\cdot\hat{s}')\hat{s}\cdot\hat{s}'d\Omega' = \frac{1}{2W_0}\int_{4\pi} p(cos\theta)cos\theta sin\theta d\theta \qquad (2)$$

The albedo W_0 is defined by

$$W_0 = \frac{1}{4\pi}\int_{4\pi} p(\hat{s}\cdot\hat{s}')d\Omega' = \frac{\sigma_s}{\sigma_a+\sigma_s} = \frac{\mu_s}{\mu_a+\mu_s} \qquad (3)$$

With this model the spatial distribution of optical radiation in a complex biological tissue, like human skin, can be obtained as a function of the laser source parameters and the dimensions and optical properties of the tissue.

4. Optical ablation of biological tissues

There are several mechanisms that may lead to optical ablation, mainly photothermal effects, photoablation, plasma-induced ablation and photodisruption (Niemz 2004, Vogel and Venugopalan 2003). Photothermal ablation is usually associated with long exposition times (Niemz 2004), for example by a continuous wave CO_2 laser (Zhang *et al* 2009). A complex model of tissue ablation should consider the mechanical properties of the biological tissue, the dominant mechanism of ablation, thermal denaturation, phase transitions or dynamical optical properties (Vogel and Venugopalan 2003). Several simplifying approaches can be assumed, from mechanistic models, such as the thermo-mechanical or the stationary state vaporization model, to heuristic models, such as the blow-off or stationary state models (Vogel and Venugopalan 2003). Steady-state heuristic models are valid for pulsed microsecond laser sources, and assume an energy density threshold for optical ablation. A blow-off model establishes a finite radiant exposure threshold for ablation starting. Material removal is assumed to begin after finishing the irradiation. These assumptions require thermal confinement, which is fulfilled in general for pulses below 100 ns (Vogel and Venugopalan 2003).

Ablation threshold models are quite extended, as the parameters can be directly measured (Hu *et al* 2001). Although some controversy remains, optical ablation of skin by nanosecond pulses can be explained by the main mechanism of plasma-induced ablation (Fang and Hu 2004). The description of the process in a broadband spectral range requires the consideration of multiphoton ionization and ionization by light absorption. All these effects can be included in a rate equation for the quasifree electron density $\rho(t)$ (Fang and Hu 2004):

$$\frac{d\rho}{dt} = \eta\rho + \left(\frac{d\rho}{dt}\right)_{mp} + \left(\frac{d\rho}{dt}\right)_{ch} - g\rho(t) \quad (4)$$

In equation 4 η is the probability rate of cascade ionization, mp stands for multiphoton ionization, ch stands for chromophore, or light absorption by species in the tissue, and g is the electron recombination rate. This expression can be particularized for skin by neglecting the last term due to the long life and diffusion times of the electrons compared with laser pulse duration, by including usual skin chromophores, and by neglecting multiphoton ionization. The equation can be solved analytically with a simple 1D diffusion approach, and a threshold value can be fixed (Fang and Hu 2004). Alternative models for the ablation threshold for a broader pulse duration range were proposed (Loesel *et al* 1996), with a rate equation, neglecting multiphoton ionization:

$$\frac{\delta\rho}{\delta t} = \tilde{\beta}\rho(t) - g\rho(t) \qquad (5)$$

In equation 5 $\tilde{\beta}$ is the reduced avalanche ionization, which takes into account inelastic collisions. The equation can be analytically solved, and a threshold value for the fluence F_{th} can be obtained (Loesel *et al* 1996):

$$\eta F_{th} = \frac{1}{2} ln\left(\frac{N_{th}}{N_0}\right) + \sqrt{\left(\frac{1}{2} ln\left(\frac{N_{th}}{N_0}\right)\right)^2 + \frac{\tau}{2\tau_c}} + \frac{\tau}{\tau_d} \quad (6)$$

This equation depends on laser pulse duration τ, the time constants for inelastic collision and diffusion τ_c and τ_d , respectively, the initial electron density N_0, and the threshold electron density N_{th}.

The present predictive models of tissue ablation consider optical propagation by either a simple one-dimensional Beer-Lambert law (Vogel and Venugopalan 2003, Zhang *et al* 2009) or an approximate one-dimensional diffusion approach (Fang and Hu 2004). All these approaches do not take into account the real three dimensional problem of optical ablation, specifically relevant due to optical scattering of radiation. A first attempt was made by the authors (Fanjul-Vélez *et al* 2013), but further analysis and results are needed.

5. Results and discussion

Three different non-melanoma skin cancer lesions were considered, SCC, BCC, and INF, whose characteristics were discussed in section 2, and healthy skin for comparison. The first step to predict possible laser ablation is the calculation of optical propagation by the Monte Carlo approach described in section 3. Laser surgery by a PDL picosecond pulsed laser at 633 nm, visible for easier medical praxis, was assumed. The optical properties of healthy skin, corresponding to a seven-layered model for healthy skin appear in table 1 (Tuchin 1993). The optical properties of SCC are estimated as refractive index $n = 1.5$, absorption coefficient $\mu_a = 2\ cm^{-1}$, scattering coefficent $\mu_s = 95.238\ cm^{-1}$, anisotropy of scattering $g = 0.79$. Those of BCC are $n = 1.5$, $\mu_a = 1.5\ cm^{-1}$, $\mu_s = 104.76\ cm^{-1}$, and $g = 0.79$. Finally the ones employed for INF are $n = 1.5$, $\mu_a = 1.5\ cm^{-1}$, $\mu_s = 142.85\ cm^{-1}$, and $g = 0.79$ (Salas-García *et al* 2012a, Salomatina *et al* 2006).

Table 1. Optical properties of the human healthy skin in a seven layered model, at 633 nm. The parameters are n, refractive index; μ_a, absorption coefficient; μ_s, scattering coefficient; g, anisotropy of scattering; d, layer thickness.

Layer	n	μ_a [1/cm]	μ_s [1/cm]	g	d [cm]
Epidermis	1.5	25	480	0.79	0.0065
Upper dermis	1.4	2.7	187	0.82	0.063
Blood plexus	1.35	25	400	0.98	0.072
Lower dermis	1.4	2.7	187	0.82	0.1285
Subcutaneous fat	1.45	0.2	20	0.8	0.1605
Vessel wall	1.37	6	414	0.91	0.2215
Blood	1.35	25	400	0.98	0.8595

Non-melanoma skin cancer lesions with a 0.3 cm thickness were considered. We analysed two different spatial profiles, Gaussian and Top hat, two different laser radii, 0.1 mm and 1 cm, and several total delivered energies. Some results of relative optical absorption are presented in figure 3.

In figure 3 optical absorption concentrates preferentially near the tissue surface in all the graphs, as expected. The penetration depth in healthy skin, figures 3a), 3b) and 3c), is in general smaller than in the non-melanoma skin cancer lesions. In figure 3b), with a Gaussian 1

mm radius laser beam, the penetration depth in healthy skin is significantly reduced compared with SCC, BCC and INF, figures 3e), 3h) and 3k), respectively. The penetration depth of SCC tumor, figure 3e), is lower than that of the INF tumor, figure 3k), for the same optical source. Optical absorption is higher as the energy increases, as can be seen by comparing figures 3a) and 3b) for healthy skin, and energies of 0.05 and 0.16 J, respectively. The same situation occurs for SCC, figures 3d) and 3e), BCC, figures 3g) and 3h), and INF, figures 3j) and 3k). Comparing figures 3e), Gaussian, and 3f), Top hat 1 cm radius, for an SCC tumor, the optical absorption has a more rectangular shape for Top hat profile. With a Top hat beam the absorption in healthy skin, figure 3c), is more concentrated near the tissue surface, while it goes deeper in tumors, figures 3f), 3i) and 3l). The absorption reaches higher values for the same depth in the BCC or INF, figures 3i) and 3l), than in the SCC, figure 3f).

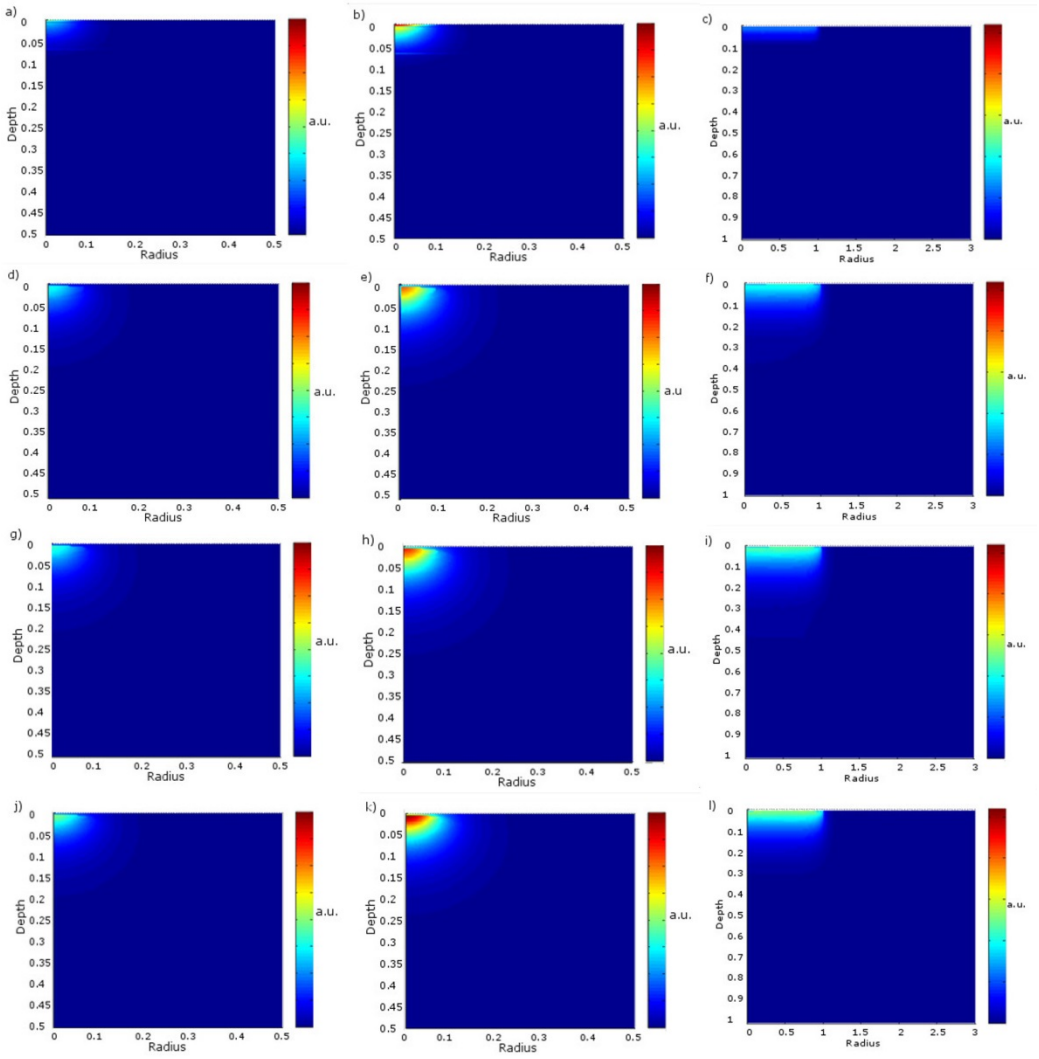

Figure 3. Optical relative absorption (arbitrary units) in healthy and tumoral skin for different parameters of the laser source at 633 nm. The representation shows 2D slices in the radial (cm) and depth (cm) directions (the center of the beam superficial impact point is at position (0,0). a) Healthy skin, Gaussian beam 1 mm radius, 0.05 J; b) Healthy skin, Gaussian beam 1 mm radius, 0.16 J; c) Healthy skin, Top hat beam 1 cm radius, 5 J; d) SCC, Gaussian beam 1mm radius, 0.05 J; e) SCC, Gaussian beam 1 mm radius, 0.16 J; f) SCC, Top hat beam 1 cm radius, 5 J; g) BCC, Gaussian beam 1mm radius, 0.05 J; h) SCC, Gaussian beam 1 mm radius, 0.16 J; i) SCC, Top hat beam 1 cm radius, 5 J; j) INF, Gaussian beam 1mm radius, 0.05 J; k) INF, Gaussian beam 1 mm radius, 0.16 J; l) INF, Top hat beam 1 cm radius, 5 J. Note the different scales of radius and depth, and the different normalization factor in colorbars in f), i) and l).

The parameters of rate equations for tissue ablation are difficult to obtain. There are results for some particular examples, either for skin epidermis in the nanosecond regime at 1064, 532,

266 and 213 nm, following the more complex method of equation 4 (Fang and Hu 2004), or for human enamel, human cornea and bovine brain, at 620 and 1053 nm, as a function of pulse duration, following equation 6, and also measured (Loesel *et al* 1996). In this work the analysis follows equation 6 for fluence threshold calculation. This threshold is experimentally corroborated on human cornea at 620 nm, a collagen-based biological tissue like the skin. For a 5 ps PDL 633 nm laser, the fluence threshold is 5 J/cm^2 (Loesel *et al* 1996).

Optical propagation results are incorporated in the ablation model. Some results of ablation areas and volumes in healthy and cancerous skin are shown in figure 4.

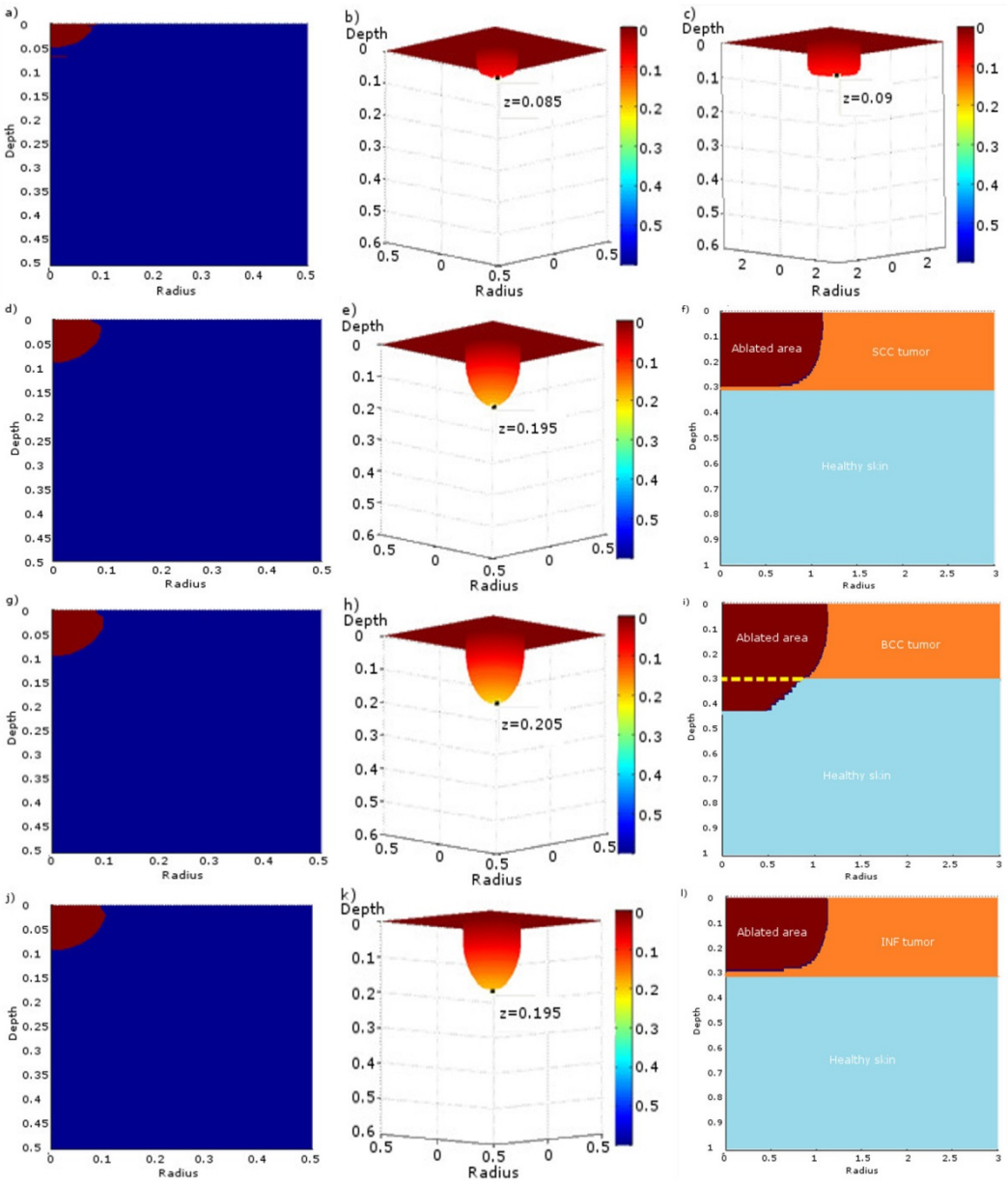

Figure 4. Results of the estimated ablation area or volume in healthy skin, SCC, BCC and INF tumors, for different laser configurations. a) Ablated area in healthy skin with a Gaussian 1 mm radius 0.16 J total energy laser beam; b) Ablated volume in healthy skin with a Gaussian 1 mm radius 1 J total energy laser beam; c) Ablated volume in healthy skin with a Top hat 1 cm radius 100 J total energy laser beam; d) Ablated area in SCC tumor with a Gaussian 1 mm radius 0.16 J total energy laser beam; e) Ablated volume in SCC tumor with a Gaussian 1 mm radius 1 J total energy laser beam; f) Ablated area in SCC tumor with a Top hat 1 cm radius 100 J total energy laser beam; g) Ablated area in BCC tumor with a Gaussian 1 mm radius 0.16 J total energy laser beam; h) Ablated volume in BCC tumor with a Gaussian 1 mm radius 1 J total energy laser beam; i) Ablated area in SCC tumor with a Top hat 1 cm radius 100 J total energy laser beam; j) Ablated area in INF tumor with a Gaussian 1 mm radius

0.16 J total energy laser beam; k) Ablated volume in INF tumor with a Gaussian 1 mm radius 1 J total energy laser beam; l) Ablated area in INF tumor with a Top hat 1 cm radius 100 J total energy laser beam. All the dimensions are in cm, in figures a), d), f), g), i), j) and l) the radiation is impinging from above at position (0,0) (upper left corner); in the rest, b), c), e), h) and k) the radiation is impinging from above at position (0,0,0) (upper center).

The maximum ablation depth is below 0.5 mm in healthy skin, figure 4a), for a Gaussian 1 mm radius laser beam, and deposition energy of 0.16 J, while in SCC, figure 4d), BCC, figure 4g) and INF, figure 4j), it is about 0.8 mm. The radial extension of the ablated area presents a maximum value of approximately 0.8 mm for healthy skin, figure 4a), and around 1 mm for the tumors, figures 4d), 4g) and 4j). If the delivered energy is increased to 1 J by longer exposition time, the maximum ablation depth increases, until around 0.85 mm in healthy skin, figure 4b), until around 1.95 mm for the SCC and INF, figures 4e) and 4k), and slightly deeper, until 2.05 mm, for the BCC tumor, figure 4h). For a Top hat 1 cm radius laser beam that delivers 100 J, the ablation depth goes to around 0.9 mm in healthy skin, figure 4c), and until almost 3 mm for SCC, figure 4f), and INF, figure 4l). In the case of a BCC tumor, figure 4i), predicted ablation depth surpasses 4 mm, so tumoral 0.3 cm tissue is completely ablated and even part of the healthy tissue, avoiding recurrence. The rest of the tumor, that extends radially, could be ablated by successive sessions of laser surgery, by displacing the laser source.

A further analysis of ablation depth, superficial area and ablation volume is shown in figure 5.

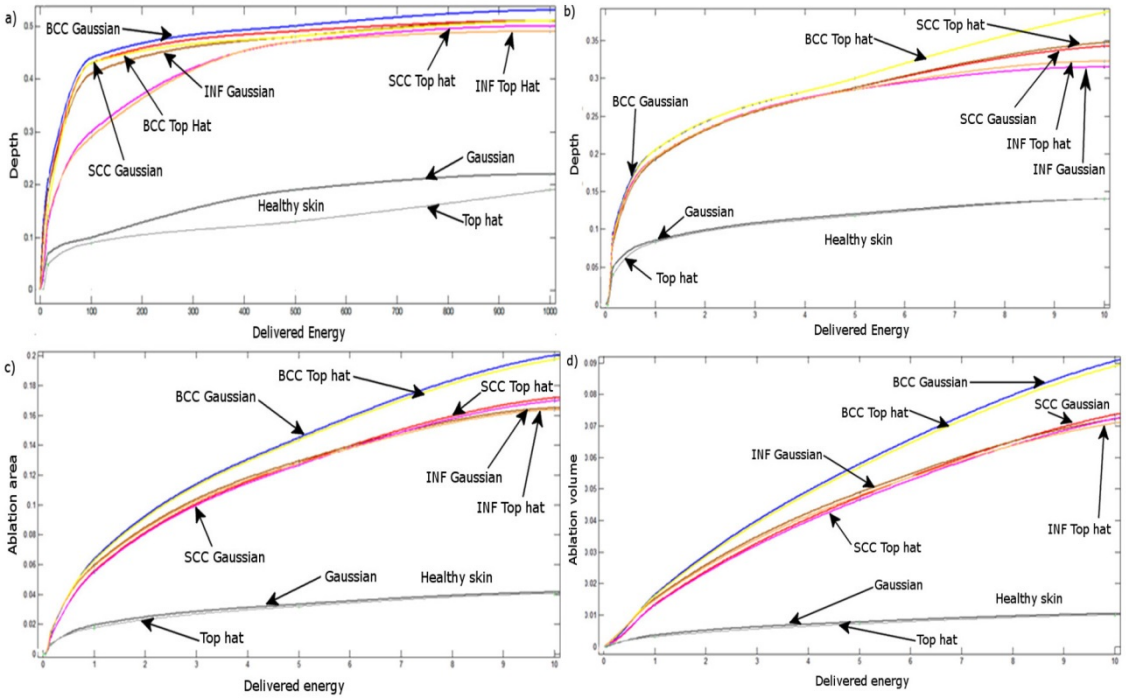

Figure 5. Ablation depth, superficial area and volume on healthy skin and SCC, BCC and INF tumors for different laser beam total delivered energy and spatial profile. a) Ablation depth (cm) as a function of total delivered energy (J) by a 1 cm radius beam of Gaussian and Top hat spatial profile; b) Ablation depth (cm) as a function of total delivered energy (J) by a 1 mm radius beam of Gaussian and Top hat spatial profile; c) Ablation area (cm2) as a function of total delivered energy (J) by a 1 mm radius beam of Gaussian and Top hat spatial profile; d) Ablation volume (cm3) as a function of total delivered energy (J) by a 1 mm radius beam of Gaussian and Top hat spatial profile.

Figures 5a) and 5b) present the maximum ablation depth as a function of the total delivered energy, for 1 cm and 1 mm radius beam, respectively, and for healthy skin and BCC, SCC and INF tumors, Gaussian and Top hat profiles. In general the ablation depth can be higher for the 1 cm radius beam by energy increasing, until above 5 mm for a BCC tumor irradiated by a

Gaussian beam, figure 5a), while values of around 4 mm can be reached with 1 mm radius, figure 5b). Healthy skin presents lower ablation depths than tumors, and the ablation depth in BCC is higher than in SCC or INF, figures 5a) and 5b). Gaussian beams lead to deeper ablation depths than Top hat profiles, with more significant differences for a 1 cm radius laser beam, figure 5a). This difference remains in healthy skin as energy increases, while it is reduced in tumors. A saturation effect with increasing energy can be appreciated in general, clearly in figure 5a), for the 1 cm radius, and also in figure 5b). This effect is related with the limited penetration depth of optical radiation in turbid media. Figures 5c) and 5d) represent the ablation area, in cm2, and volume, in cm3, respectively, for a 1 mm radius laser beam, with Gaussian or Top hat spatial profile, in healthy skin and BCC, SCC and INF tumors, as a function of the total delivered energy. Again the ablation on healthy skin is smaller than on tumors. The ablation area and volume are larger in BCC than in SCC or INF lesions. Gaussian profile induces slightly larger ablation areas and volumes when compared with Top hat. The results of ablation depth, area and volume are consistent with each other.

The results of this section show clearly the relevance of choosing adequate laser beam parameters for a laser surgery session, as a function of the type of lesion, the patient and the aim of the surgical procedure. The ablation depth, area and volume can change significantly for different lesions, and could be even personalized for the lesion of a particular patient, by measuring the optical properties. The ablation threshold should also be adjusted for a totally personalized procedure. A saturation effect was observed in ablation depth, so there is a limit in the total amount of tumoral tissue that can be removed. However, there is a possibility of repeating the surgical procedure in successive sessions, so the ablation depth would increase. Of course new predictions should be made in this case for achieving an appropriate resected volume.

6. Conclusions

The application of laser surgery, either for tissue ablation or for malignant tumor resection, requires an adequate knowledge of laser beam and biological tissue characteristics to optimize the procedure. We have proposed a novel predictive tool for tissue ablation in biological tissues that allows the a priori estimation of the ablation depth, area and volume. The 3D approach is based on a Monte Carlo method for optical propagation in biological tissues, and a rate equation for plasma-induced ablation. Previous models did not consider the complex propagation behavior of light in tissue, nor the 3D character of the problem. The tool is lesion-sensitive, as the geometric, optical and ablation properties of the specific biological tissue are employed. It allows also the consideration of variations in laser beam radius, spatial profile, pulse width, total delivered energy or wavelength. The predictive tool is applied in dermatology, particularly in healthy skin and different types of non-melanoma skin cancer tumors: BCC, SCC and INF. The optical source is considered to be a PDL laser. Several predictions are made by varying the optical beam parameters and tumor type. The results show an estimation of the ablation volume, ablation area and ablation depth, for each case. The model allows the adjustment of the laser beam parameters for complete tumor resection. In case several sessions are required, the tool could consider also the subsequent sessions by changing the parameters according to the new situation. This tool could be useful for laser surgery planning, prior to the clinical application of the procedure. Better results of volume resection could be obtained, as its application would be personalized to the particular patient and lesion.

Acknowledgements

This work has been partially supported by the project MAT2012-38664-C02-01 of the Spanish Ministery of Economy and Competitiveness, and by San Cándido Foundation. We would also like to thank the Dermatology Department of the Marqués de Valdecilla University Hospital for providing the images and clinical data of lesions.

References

Alexandrescu DT, Ross EV 2012 New Frontiers in Laser Surgery *Seminars in Cutaneous Medicine and Surgery* **31** 88-97

Bohren CF, Huffman DR 1983 *Absorption and Scattering of Light by Small Particles* John Wiley & Sons USA

Choudhary S, Tang J, Elsaie ML, Nouri K. 2011 Lasers in the Treatment of Nonmelanoma Skin Cancer *Dermatologic Surgery* **37** 409-425

Diepgen TL, Mahler V 2002 The Epidemiology of Skin Cancer *British Journal of Dermatology* **146** 1-6

Fang Q, Hu XH 2004 Modeling of Skin Tissue Ablation by Nanosecond Pulses From Ultraviolet to Near-Infrared and Comparison with Experimental results *IEEE Journal of Quantum Electronics* **40** 69-77

Fanjul-Vélez F, Arce-Diego JL 2008 Modeling thermotherapy in vocal cords novel laser endoscopic treatment *Lasers in Medical Science* **23** 169–177

Fanjul-Vélez F, Blanco-Gutiérrez A, Salas-García I, Ortega-Quijano N, Arce-Diego JL 2013 Predictive analysis of optical ablation in several dermatological tumoral tissues *Proceedings of SPIE* **8803** 8803R1

Fanjul-Vélez F, Salas-García I, Fernández-Fernández LA, López-Escobar M, Buelta-Carrillo L, Ortega-Quijano N, Arce-Diego JL 2009a Photochemical model of Photodynamic Therapy applied to skin diseases by a topical photosensitizer *Proceedings of SPIE* **7373** 73730S

Fanjul-Vélez F, Romanov OG, López-Escobar M, Ortega-Quijano N, Arce-Diego JL 2009b Necrosis prediction of Photodynamic Therapy applied to skin disorders *Proceedings of SPIE* **7161** 71610P

Hu XH, Fang Q, Cariveau MJ, Pan X, Kalmus GW 2001 Mechanism study of porcine skin ablation by nanosecond laser pulses at 1064, 532, 266, and 213 nm *IEEE Journal of Quantum Electronics* **37** 322-328

Loesel FH, Niemz MH, Bille JF, Juhasz T 1996 Laser-Induced Optical Breakdown on Hard and Soft Tissues and Its Dependence on the Pulse Duration: Experiment and Model *IEEE Journal of Quantum Electronics* **32** 1717-1722

Niemz MH 2004 *Laser-Tissue Interactions Fundamentals and Applications* Springer Germany

Peng Q, Juzeniene A, Chen J, Svaasand LO, Warloe T, Giercksky KE, Moan J 2008 Lasers in medicine *Reports on Progress in Physics* **71** 1-28

Salas-García I, Fanjul-Vélez F, Arce-Diego JL 2012a Influence of the Human Skin Tumor Type in Photodynamic Therapy Analysed by a Predictive Model *International Journal of Photoenergy* **2012** 1-9

Salas-García I, Fanjul-Vélez F, Arce-Diego JL 2012b Photosensitizer absorption coefficient modeling and necrosis prediction during photodynamic therapy *Journal of Photochemistry and Photobiology B:Biology* **114** 79-86

Salomatina E, Jiang B, Novak J, Yaroslavsky AN 2006 Optical properties of normal and cancerous human skin in the visible and near-infrared spectral range *Journal of Biomedical Optics* **11** 0640261–640269

Sankaranarayanan G, Resapu RR, Jones DB, Schwaitzberg S, De S 2013 Common uses and cited complications of energy in surgery *Surgical Endoscopy* **27** 3056-3072

Tuchin VV 1993 Laser light scattering in biomedical diagnostics and therapy *Journal of Laser Applications* **5** 43–60

Vo-Dinh T 2003 *Biomedical Photonics Handbook* CRC Press Boca Raton

Vogel A, Venugopalan V 2003 Mechanisms of Pulsed Laser Ablation of Biological Tissues. Chemical Reviews 103:577-644

Wang L, Jacques SL, Zheng L 1995 MCML – Monte Carlo modeling of light transport in multi-layered tissues *Computer methods and programs in biomedicine* **47** 131-146

Zhang JZ, Shen YG, Zhang XX 2009 A dynamic photo-thermal model of carbon dioxide laser tissue ablation *Lasers in Medical Science* **24** 329-338

Figure captions

Figure 1. Images of Basal Cell Carcinomas (BCC). Marqués de Valdecilla University Hospital.

Figure 2. Images of actinis keratosis (left) and Bowen disease (right). Marqués de Valdecilla University Hospital.

Figure 3. Optical relative absorption (arbitrary units) in healthy and tumoral skin for different parameters of the laser source at 633 nm. The representation shows 2D slices in the radial (cm) and depth (cm) directions (the center of the beam superficial impact point is at position (0,0). a) Healthy skin, Gaussian beam 1 mm radius, 0.05 J; b) Healthy skin, Gaussian beam 1 mm radius, 0.16 J; c) Healthy skin, Top hat beam 1 cm radius, 5 J; d) SCC, Gaussian beam 1mm radius, 0.05 J; e) SCC, Gaussian beam 1 mm radius, 0.16 J; f) SCC, Top hat beam 1 cm radius, 5 J; g) BCC, Gaussian beam 1mm radius, 0.05 J; h) SCC, Gaussian beam 1 mm radius, 0.16 J; i) SCC, Top hat beam 1 cm radius, 5 J; j) INF, Gaussian beam 1mm radius, 0.05 J; k) INF, Gaussian beam 1 mm radius, 0.16 J; l) INF, Top hat beam 1 cm radius, 5 J. Note the different scales of radius and depth, and the different normalization factor in colorbars in f), i) and l).

Figure 4. Results of the estimated ablation area or volume in healthy skin, SCC, BCC and INF tumors, for different laser configurations. a) Ablated area in healthy skin with a Gaussian 1 mm radius 0.16 J total energy laser beam; b) Ablated volume in healthy skin with a Gaussian 1 mm radius 1 J total energy laser beam; c) Ablated volume in healthy skin with a Top hat 1 cm radius 100 J total energy laser beam; d) Ablated area in SCC tumor with a Gaussian 1 mm radius 0.16 J total energy laser beam; e) Ablated volume in SCC tumor with a Gaussian 1 mm radius 1 J total energy laser beam; f) Ablated area in SCC tumor with a Top hat 1 cm radius 100 J total energy laser beam; g) Ablated area in BCC tumor with a Gaussian 1 mm radius 0.16 J total energy laser beam; h) Ablated volume in BCC tumor with a Gaussian 1 mm radius 1 J total energy laser beam; i) Ablated area in SCC tumor with a Top hat 1 cm radius 100 J total energy laser beam; j) Ablated area in INF tumor with a Gaussian 1 mm

radius 0.16 J total energy laser beam; k) Ablated volume in INF tumor with a Gaussian 1 mm radius 1 J total energy laser beam; l) Ablated area in INF tumor with a Top hat 1 cm radius 100 J total energy laser beam. All the dimensions are in cm, in figures a), d), f), g), i), j) and l) the radiation is impinging from above at position (0,0) (upper left corner); in the rest, b), c), e), h) and k) the radiation is impinging from above at position (0,0,0) (upper center).

Figure 5. Ablation depth, superficial area and volume on healthy skin and SCC, BCC and INF tumors for different laser beam total delivered energy and spatial profile. a) Ablation depth (cm) as a function of total delivered energy (J) by a 1 cm radius beam of Gaussian and Top hat spatial profile; b) Ablation depth (cm) as a function of total delivered energy (J) by a 1 mm radius beam of Gaussian and Top hat spatial profile; c) Ablation area (cm^2) as a function of total delivered energy (J) by a 1 mm radius beam of Gaussian and Top hat spatial profile; d) Ablation volume (cm^3) as a function of total delivered energy (J) by a 1 mm radius beam of Gaussian and Top hat spatial profile.